DOT/FAA/AR-08/6

Air Traffic Organization
Operations Planning
Office of Aviation Research
Washington, DC 20591

Tests and Interpretation of Small Fatigue Crack Growth in Metallic Rotorcraft Structures With Emphasis on the Statistical Characteristics

February 2008

Final Report

This document is available to the U.S. public through the National Technical Information Service (NTIS), Springfield, Virginia 22161.

U.S. Department of Transportation
Federal Aviation Administration

NOTICE

This document is disseminated under the sponsorship of the U.S. Department of Transportation in the interest of information exchange. The United States Government assumes no liability for the contents or use thereof. The United States Government does not endorse products or manufacturers. Trade or manufacturer's names appear herein solely because they are considered essential to the objective of this report. This document does not constitute FAA certification policy. Consult your local FAA aircraft certification office as to its use.

This report is available at the Federal Aviation Administration William J. Hughes Technical Center's Full-Text Technical Reports page: actlibrary.tc.faa.gov in Adobe Acrobat portable document format (PDF).

Technical Report Documentation Page

1. Report No.	2. Government Accession No.	3. Recipient's Catalog No.
DOT/FAA/AR-08/6		

4. Title and Subtitle	5. Report Date
TESTS AND INTERPRETATION OF SMALL FATIGUE CRACK GROWTH IN METALLIC ROTORCRAFT STRUCTURES WITH EMPHASIS ON THE STATISTICAL CHARACTERISTICS	February 2008
	6. Performing Organization Code
7. Author(s)	8. Performing Organization Report No.
Marcus D. Cappelli, Robert L. Carlson, and George A. Kardomateas	
9. Performing Organization Name and Address	10. Work Unit No. (TRAIS)
Georgia Institute of Technology School of Aerospace Engineering Atlanta, GA 30332	
	11. Contract or Grant No. NGT 2-52274
12. Sponsoring Agency Name and Address	13. Type of Report and Period Covered
U.S. Department of Transportation Federal Aviation Administration Air Traffic Organization Operations Planning Office of Aviation Research and Development Washington, DC 20591	Final Report
	14. Sponsoring Agency Code ASW-112

15. Supplementary Notes

The Federal Aviation Administration Airport and Aircraft Safety R&D Division COTR was Dy Le.

16. Abstract

This report presents the results of an experimental program on the growth of small, multisite fatigue cracks on smooth surfaces in 7075-T7351 aluminum. It was shown that the resulting population of measured cracks was bimodal. That is, it consisted of primary cracks that can grow until failure by fracture in each specimen, and secondary cracks that ultimately arrest. An experimental procedure for separating the two distributions was developed and used to obtain confidence intervals for crack length versus loading cycles. A microstructurally based transition point between small and long crack behavior was also developed and used. Topics for additional research that need to be further developed and applied to the bimodal model of cluster small crack growth are presented.

17. Key Words	18. Distribution Statement
Small cracks, Clusters, Bimodal distribution	This document is available to the U.S. public through the National Technical Information Service (NTIS), Springfield, Virginia 22161.

19. Security Classif. (of this report)	20. Security Classif. (of this page)	21. No. of Pages	22. Price
Unclassified	Unclassified	26	

Form DOT F 1700.7 (8-72) Reproduction of completed page authorized

ACKNOWLEDGMENTS

A team that included both school faculty and students completed the work for this project. Both co-principal investigators are faculty members of the Georgia Institute of Technology, School of Aerospace Engineering. Professor George Kardomateas works at the institute full time, while Professor Robert Carlson is a Professor Emeritus.

Several students also contributed to the project. The majority of the laboratory work, presentations, and paper writing was completed by Marcus Cappelli. Marcus was a Ph.D. candidate in aerospace. A second graduate student who assisted on the project was Wendy Hynes. Wendy was awarded a Masters in aerospace in 2006 and has worked as a full-time Senior Engineer at Lockheed Martin throughout her time at the school. Both graduate students were assisted by several undergraduate students who, through their work in the laboratory, gained much experience and knowledge. These students were Christopher Neglia, Heinrich Souza, Varun Sharma, Terry Williams, and John Hamil.

TABLE OF CONTENTS

		Page
EXECUTIVE SUMMARY		ix
1.	INTRODUCTION	1
1.1	Objective	1
1.2	Background	1
2.	DISCUSSION	1
3.	EVALUATION APPROACH	5
3.1	Material Summary	5
3.2	Test Specimen	6
3.3	Test Setup	7
3.4	Data	7
3.5	Analysis	8
3.5.1	Bimodal Model	8
3.5.2	Confidence Limit Analysis	11
3.5.3	Cluster Effects and Measurements	14
3.6	Recommendations for Continuing Research	16
3.6.1	Operational Issues	16
3.6.2	Analysis	16
3.6.3	Alternate Materials	16
4.	CONCLUSIONS	17
5.	REFERENCES	18

LIST OF FIGURES

Figure		Page
1	Corner Micronotch Specimen Geometry	2
2	Crack Growth Rate vs Crack Length	3
3	Crack Growth Rate Standard Deviation/Grain Intersections vs Crack Length	3
4	Sample Crack Geometries and Standard Deviation of Crack Growth Rate vs Grain Intersections	5
5	Material Microstructure: Longitudinal and Short Transverse	6
6	Specimen Geometry	7
7	Common Crack Shapes	8
8	Assumed Geometry of Cracks	9
9	Crack Growth Rates in Both Small and Long Regimes	10
10	Crack Length vs Cycle Count for All Cracks Measured on Specimen F	11
11	Confidence Bounds on the Mean of the Crack Lengths as Well as Primary Crack Data	13
12	Confidence Bounds With the Inclusion of Secondary Cracks	14
13	Topology of Multisite Crack Growth Through the Life of a Specimen	15
14	Microstructure of Ti-6Al-4V With Increased Cooling Rates and Finer Structures Towards the Right	17

LIST OF TABLES

Table		Page
1	Average Grain Dimensions	2
2	Material Properties	5
3	Material Grain Dimensions	6

EXECUTIVE SUMMARY

A considerable part of the total fatigue life in rotorcraft structures can be spent in the small crack growth regime. Small crack growth characteristics are unlike those for medium to long-sized cracks. They include a growth-arrest mechanism, coalescence of microcracks, and growth that can occur at smaller stress-intensity factors than for nominally equivalent long cracks. A very prominent feature of small fatigue crack growth is the scatter, which is significantly greater than for long cracks.

The growth and scatter of small, multisite fatigue cracks on smooth surfaces is the topic of this research. On a smooth surface, small fatigue cracks will initiate and grow in clusters. This study shows how the distribution of cracks in clusters is bimodal and can be separated into two statistical distributions. The first distribution is primary cracks, which may grow, possibly through coalescence, to cause specimen or component failure. The second distribution consists of secondary cracks that will ultimately arrest and create a unique background through which primary cracks must grow. In this report, the results of a test program on crack clusters, such as the data in 7075-T7351 aluminum alloy, are presented. An experimental method for separating the two distributions is also presented and used to conduct a proper statistical analysis on the data that quantifies the inherent measured scatter (such as the proper confidence intervals for crack length versus loading cycles).

Larger than normal amounts of scatter in crack growth rates were observed in the growth of small cracks. To better quantify the small crack regime of fatigue crack growth, a microstructurally based transition point between long and small crack behavior was developed. This work used previous research completed on small cracks grown from micronotches. This transition point was then applied to the current test data and shows that, as cracks grow past this characteristic length, their behavior changes markedly.

In addition to the current work, recommendations for continuing research are discussed. This research extended the use of the bimodal model of cluster cracking to be applied to various additional metallic materials as well as operational conditions. The continued research should include topics such as the effects of complex material microstructure on the growth of small fatigue crack clusters in Ti-6Al-4V and operational issues such as varying *R*-Ratio, variable amplitude loading, and surface finish effects.

1. INTRODUCTION.

1.1 OBJECTIVE.

The objective of this research was to present the basic experimental results of a bimodal, statistical representation of the scatter of both primary and secondary crack lengths as functions of loading cycle, as conducted under Federal Aviation Administration Grant NGT 2-52274.

1.2 BACKGROUND.

Scatter in fatigue crack growth originates during the crack initiation and the small crack growth phases. Schijve [1] has provided descriptions of both the different operative crack initiation mechanisms and the salient features of small fatigue crack growth. Changes in statistical crack size distributions with increasing load cycles were previously examined by Chen, Sauer, Meshi, and Tucker [2], and by Stolarz and Kurzydlowski [3].

Swain [4] examined multisite cracking and proposed criteria for identifying what were described as valid and invalid cracks within the clusters of small cracks. In the terminology used here, the valid cracks were described as primary cracks; these are the cracks in each specimen that can grow until failure by fracture. The invalid cracks are described as secondary cracks; these ultimately arrest or coalesce with primary cracks. The primary cracks cannot be identified easily during the early crack growth phase. The selection process requires the use of Swain's criteria [4], that is, the growth histories of all the cracks in each specimen must be measured and recorded until an identification of the primary crack emerges.

As long as a primary crack, which may be the result of crack coalescence, is within the region of influence of the secondary cracks, it can be expected to be subject to shielding effects. The networks of the secondary cracks, along with the grain boundaries, therefore, form the neighborhood within which each primary crack grows. Since the networks of secondary cracks can introduce shielding effects, they may have an influence on the driving force for the growth of the primary cracks.

The consequences of partitioning the multisite cracks into primary and secondary groups can be shown by a consideration of tests on multiple structural elements or specimens. Each separate specimen or structural element with multisite cracking will have a total of m primary cracks and n secondary cracks, for a total of (m+n) cracks. For all the elements, there are two distinct sample distributions. It follows that the total population is bimodal. The statistical analysis performed in the current investigation places emphasis on the primary crack distribution of the total population, because it is those cracks that can ultimately lead to failure by fracture.

2. DISCUSSION.

Studies on small cracks, which provide a basis for the separation crack of the distributions of multisite cracks in the current work, was previously conducted at the Georgia Institute of Technology, School of Aerospace Engineering by Carlson and Kardomateas [5]. In this project, cracks were grown from micronotches in specimens cut from 6061-T651 aluminum alloy in rod form. The specimen geometry, which contained a square cross section, is shown in figure 1.

The micronotches were cut into two opposing corner edges of the specimen, using a digitally controlled slitting saw to a depth of 150 microns. Loading to a maximum stress of 80% of the yield strength was conducted by bending about the cross section diagonal, not containing the notches, at a frequency of 10 Hz. A metallographic analysis provided the average grain dimensions, which are shown in table 1.

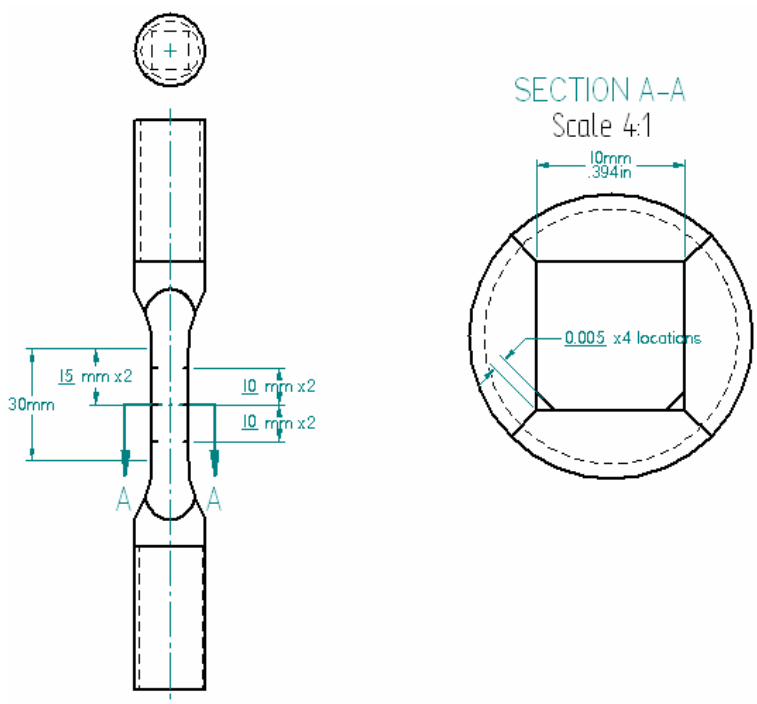

Figure 1. Corner Micronotch Specimen Geometry

Table 1. Average Grain Dimensions

Longitudinal	Transverse
350 microns	200 microns

A cubic regression was performed on the crack length (a) versus loading cycles (N) data, and the resulting equations were differentiated to provide the crack growth rate versus loading cycle. These data are presented in figure 2.

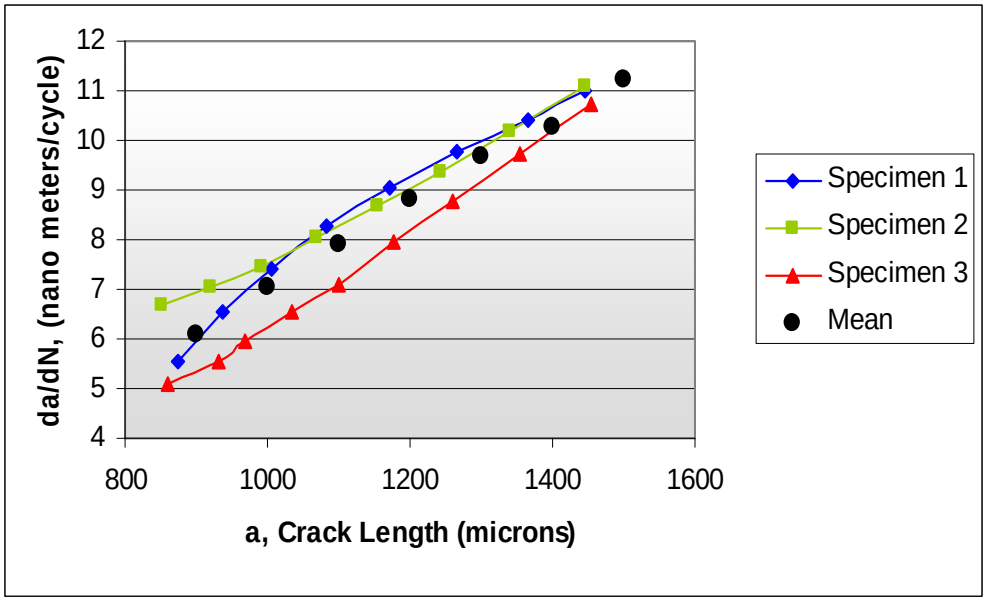

Figure 2. Crack Growth Rate vs Crack Length

A plot of the standard deviation of the crack growth rates versus crack length is provided in figure 3. The corner crack front was assumed to be a quarter arc of a circle. Metallographic examinations of fractured surfaces confirmed this to be a valid assumption. The number of grains intersected by the crack front is then given by the equation $n = 0.5\pi\ (a/d)$, where a is the crack depth and d is the average grain diameter. A second plot shows the number of grains, n, intersected by the crack fronts versus the crack length.

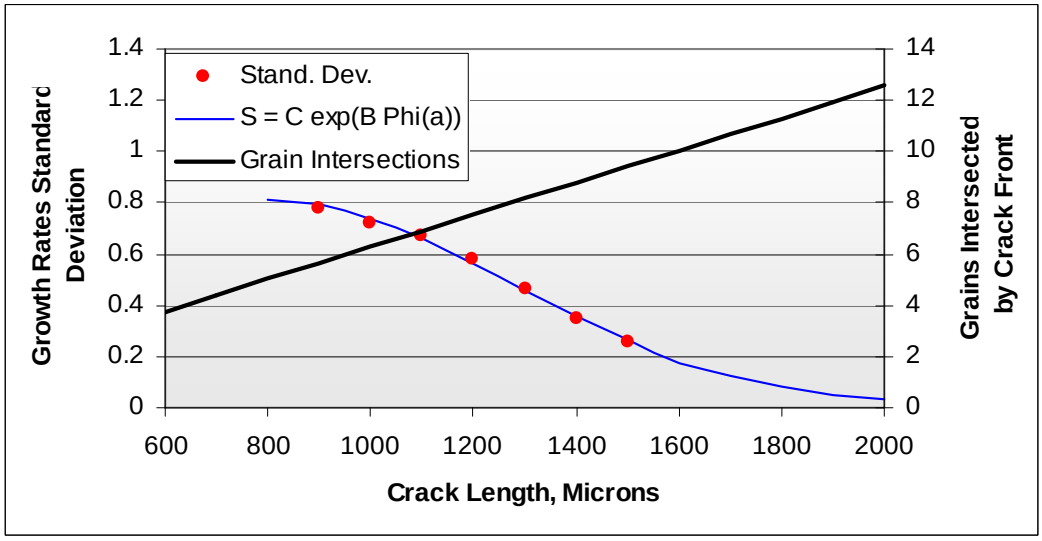

Figure 3. Crack Growth Rate Standard Deviation/Grain Intersections vs Crack Length

The trend of the data indicates that, initially, the rate of decrease in the standard deviation increases with increasing crack length. Ultimately, however, the rates of decrease begin to decrease with increasing crack length. This behavior is reasonable because it would be expected that the standard deviation should tend to approach an asymptotic value as the long crack regime is approached.

The features of the standard deviation shown in figure 3 indicate that it is possible to represent the observed behavior by an exponential function of the form:

$$S = Ce^{D(a)} \tag{1}$$

where S is the standard deviation, a is the crack length, and C and D are constants. The constants were determined by the application of a nonlinear regression analysis [6] and provided the final form of the equation shown below.

$$S = 0.81e^{\left[-2.299\cdot 10^{-6}(a-800)^2\right]} \tag{2}$$

The linear relation between a and n indicates that S can also be represented as a function of n. The resulting substitution was used to obtain the plot in figure 4. This version provides a basis for anticipating differences in the evolution of scatter for different crack surface shapes and microstructural textures. For example, for the same crack depth, as shown in figure 4(a) and (b), the crack front of a semicircular crack intersects twice as many grains as a corner crack. The scatter for the semicircular may, therefore, diminish more rapidly than that of a corner crack. When counting the grains intersected by the crack front, it is necessary to only include those grains through which the crack is actively growing. An example where this will become necessary is shown in figure 4(c). This crack geometry is experienced during growth into the decreasing stress field associated with bending about an axis. This crack could only grow outward towards the sides. Therefore, only these grain intersections should be counted.

From figure 4, it is apparent that after the crack fronts have intersected approximately 13 grains, the standard deviation of the crack growth rates becomes exceedingly small, below 0.2. This signifies that the cracks have become long cracks that can be treated deterministically using fracture mechanics principles. This microstructurally defined point can then be defined as the transition point from small to long crack behavior. It is this result that will be used in current work where its applicability will first be shown for a different material.

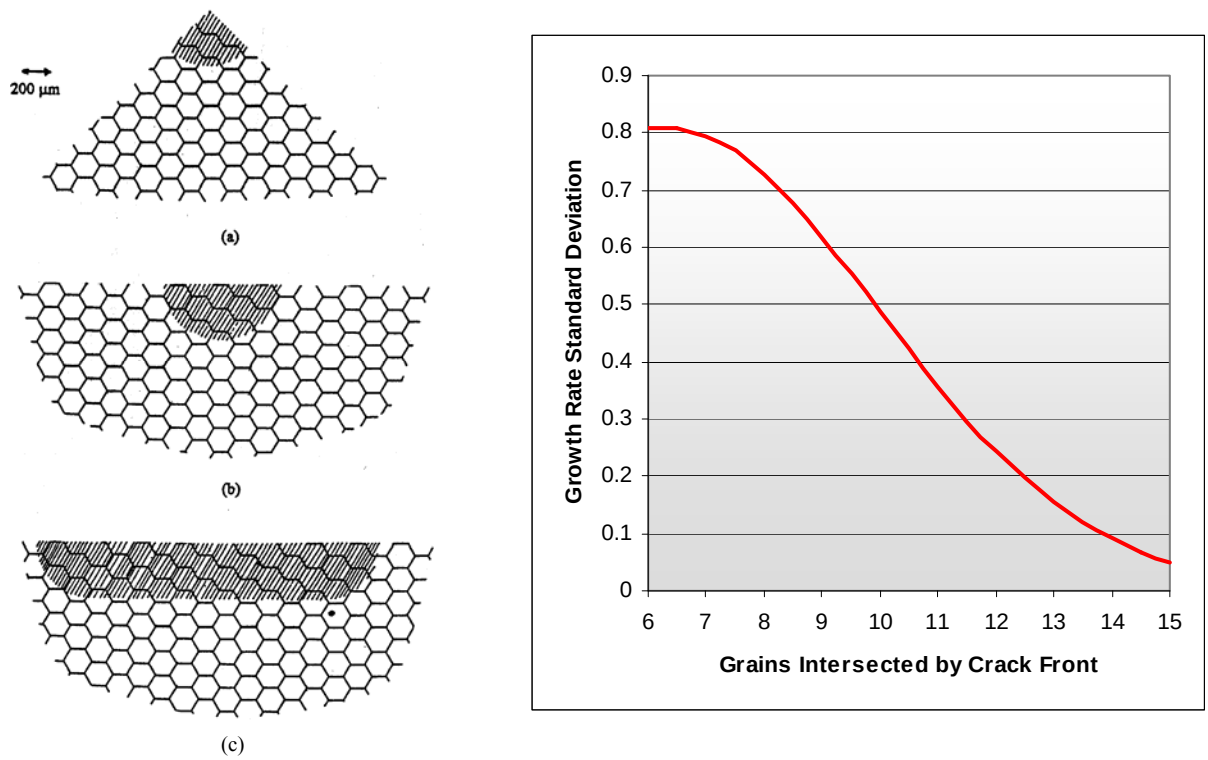

Figure 4. Sample Crack Geometries (Left) and Standard Deviation of Crack Growth Rate vs Grain Intersections (Right)

3. EVALUATION APPROACH.

3.1 MATERIAL SUMMARY.

All test specimens were machined from 7075-T7351 aluminum alloy. The material was purchased in the form of a 0.25-inch-thick plate with the mean properties shown in table 2.

Table 2. Material Properties

$\sigma_{yield\ (ksi)}$	$\sigma_{ultimate\ (ksi)}$
64	75.3

A metallographic analysis was performed by the Georgia Institute of Technology to characterize the material microstructure [7].

The microstructural texture could be described as pancake like, which is often found in plate form materials due to the rolling required. The three representative mean linear intercept grain dimensions are summarized in table 3.

Table 3. Material Grain Dimensions

Longitudinal*	Transverse*	Short Transverse*
58.8	76.1	15

*All dimensions in microns

Unlike the other measurements, the transverse grain dimension varied widely about its mean of 76.1 microns. Micrographs of two of the material directions are shown in figure 5 to emphasize the differences in the grain shape with material direction. In both graphs, the specimen's surface was etched with Keller's reagent to expose all grain boundaries. The dark spots consist of several types of intermetallic particles such as Mg_2Si and FeAl. These particles varied in size (maximum diameter) from approximately 4 to 24 microns with the vast majority falling below 10 microns.

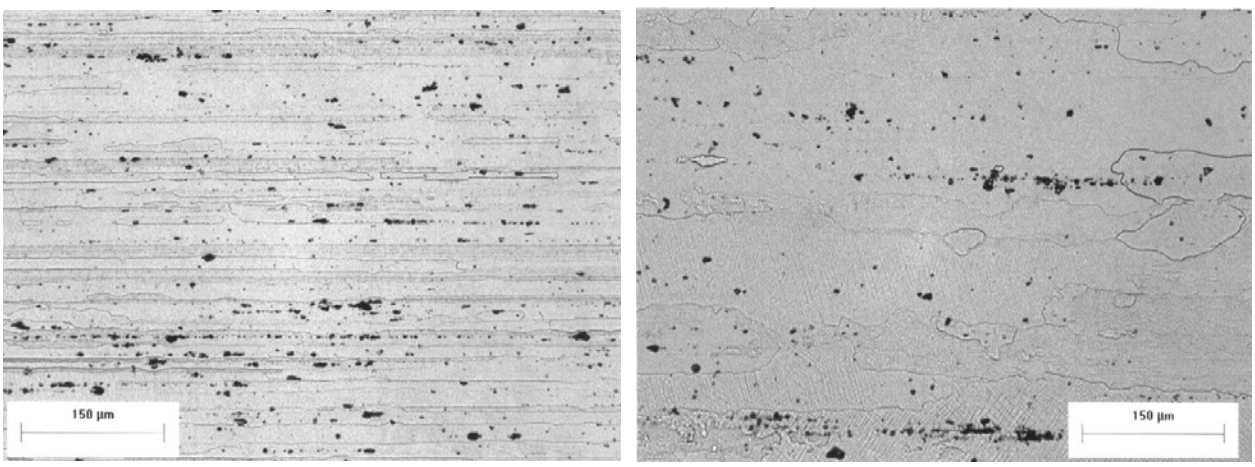

Figure 5. Material Microstructure: Longitudinal (Left) and Short Transverse (Right)

3.2 TEST SPECIMEN.

A total of 12 specimens were cut from the 0.25-inch plate. The specimen geometry is shown in figure 6. This geometry provides a moderate stress concentration factor in the reduced section of 1.2 over the ligament stress [8]. Each specimen provided two test surfaces where clusters of cracks were grown and monitored.

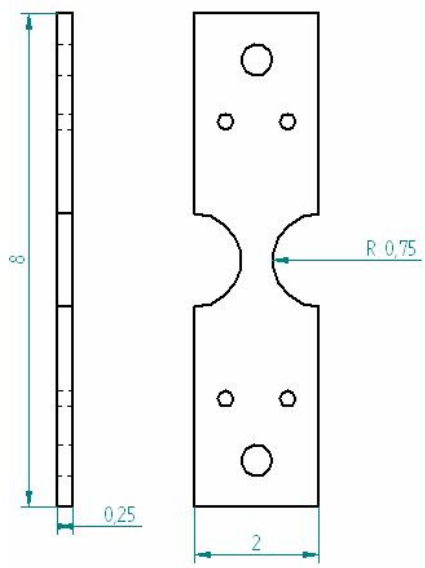

Figure 6. Specimen Geometry (All dimensions in inches)

Prior to use, all specimen gauge sections were prepared using three abrasive papers of the following grits: 240, 320, and 600. This treatment removed any surface imperfections and scratches introduced during machining. Preparation was completed by a careful polishing procedure using 15-, 6-, and 1-micron diamond pastes. This level of polishing was needed to provide a smooth surface so cracks could easily be seen with the optical sensing equipment.

3.3 TEST SETUP.

All tests were run on a digitally controlled Instron® hydraulic test stand. Both hydraulic and custom-made mechanical grips were used. No discrepancies were found in the data for the different gripping methods. The load form was sinusoidal with a frequency of 20 Hz. A maximum load of approximately 5000 lb was used, leading to a maximum stress of 75% of the material yield strength. Combined with an *R* ratio of 0.1, this led to fatigue lives on the order of 70,000 cycles that could be spanned in a reasonable amount of time.

Crack measurements were taken using a Questar telemicroscope at regular intervals throughout the life of each specimen. It is important to note that not only crack lengths were measured, but the location and shape of each crack in each cluster on both test surfaces were also carefully measured and recorded. All tests were continued until specimen failure.

3.4 DATA.

Over the span of the program, a total of 57 cracks were measured. Of these cracks, 14 were determined to be primary cracks with the remaining belonging to the secondary crack distribution. Each crack was given a two-character designation in the following manner: the first character represented the name of the specimen and the second identified the particular crack. Cracks with numerical identifiers grew on one side, while those with letters grew on the opposite.

Crack measurements were started at 40,000 cycles. Through experimentation, it was found that the first cracks would initiate and become viewable around this cycle count. The number of cycles between subsequent crack measurements was not the same for all specimens. At first cracks were measured every 5000 cycles; however, to get smoother crack length versus cycle curves, this value was reduced to 2500 cycles. This provided a balance between the amount of data generated and the time required to run a test.

Not all of the cracks measured were nominally straight. Many complex crack shapes were observed, several of them due to crack coalescence. The most common shapes seen are shown in figure 7. For each crack shape, a proper method of assigning a proper length to each crack was determined and used in the statistical analyses. They are shown in their early stages and after growth had taken place. It is often the case, such as in a forked crack, that some features of the crack growth will not grow and, thus, become insignificant as the crack becomes larger.

Name	Stage 1	Stage 2	Description
Forked Crack	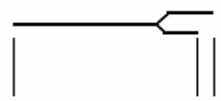	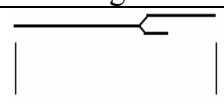	• One-fork arrests, one grows • Length is length to longer fork
Kinked Crack	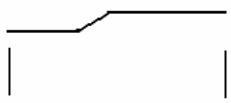	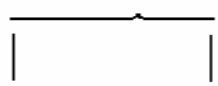	• Formed through coalescence • Tabulated as one crack after coalescence
Stepped Crack			• Formed through coalescence, which does not always occur • Tabulated as one crack after coalescence

Figure 7. Common Crack Shapes

3.5 ANALYSIS.

3.5.1 Bimodal Model.

As discussed above, the total population of cracks on a smooth surface consists of two subpopulations, primary cracks and secondary cracks. The secondary cracks generally arrest completely or grow with vanishingly low rates. This arrest can occur when a small crack intersects a microstructural feature, such as a grain boundary, which does not have enough driving force to grow through. The primary cracks are those which continue to grow and can

possibly lead to failure. Many times primary cracks grow through coalescence with other cracks in their vicinity. These cracks can grow to large lengths quickly and lead to premature failure.

Only the primary cracks should be included in any analysis since it is only these cracks that can lead to failure. The secondary cracks simply form a neighborhood that the primary cracks must grow through. Any analysis that fails to separate out the smaller secondary cracks will lead to nonconservative results. This effect is discussed below.

It was expected that the visual crack measurements used in the current experiments would miss a proportion of the cracks. However, only small secondary cracks were missed, as the primary cracks always grow large enough to be detected. These secondary cracks were separated from the primary crack distribution before analysis, therefore failing to detect some secondary cracks was inconsequential.

The two distributions of cracks could not be separated until significant crack growth had occurred and was tracked. In the early stages of crack growth, all cracks looked similar. It was only after the cracks had a chance to grow that their relative behaviors could be observed.

A simple method that makes use of entire crack growth histories was developed to determine to which distribution a crack belonged based on its relative behavior. The procedure is twofold: (1) all cracks that became microstructurally long by specimen failure are considered to be primary cracks and (2) the growth histories of cracks that are close to this boundary are investigated in more depth. If the growth rates are rising as the crack grows, like primary cracks, they are included in that distribution. If the growth rates are tending towards arrest, they are considered to be secondary cracks.

The transition point between long and short crack growth is defined using the analysis from the corner crack experiments described above. It is assumed that cracks became long after their fronts intersect on an average of 14 grains. The crack fronts are assumed to be semicircular as shown in figure 8, an assumption that was backed up by analysis of failed specimens.

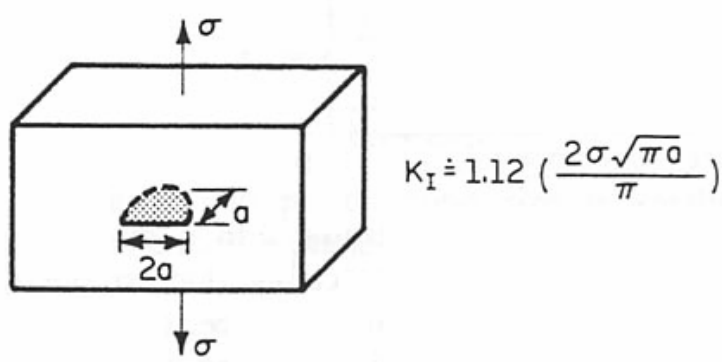

Figure 8. Assumed Geometry of Cracks

This assumption on crack shape led to the following formula for the average number of grains intersected by the crack front:

$$n = \frac{\pi 2a}{d} \tag{3}$$

In this formula, $2a$ is the crack length, and d is the average size of grains that the crack front is growing through. For the plate material under consideration and the orientation the specimens were machined from, this average grain size was an average between the longitudinal and short transverse dimensions. In the transition crack length, when the crack front intersects 13 grains, the crack becomes 0.0185 inch.

This transition length is shown in figure 9. This plot shows the crack growth rates of several representative primary cracks. The data on the left shows the small crack regime, while the data on the right shows the long crack regime. As expected, in the small crack regime, there is significant scatter, as well as the growth-arrest behavior normally associated with the growth of microstructurally small cracks. Some degree of scatter is still evident in the long crack regime; however, this is a normal scatter that will be seen with any crack measurements. It is important to note that the behavior of the cracks becomes significantly more uniform as they become predictable long cracks after the transition point.

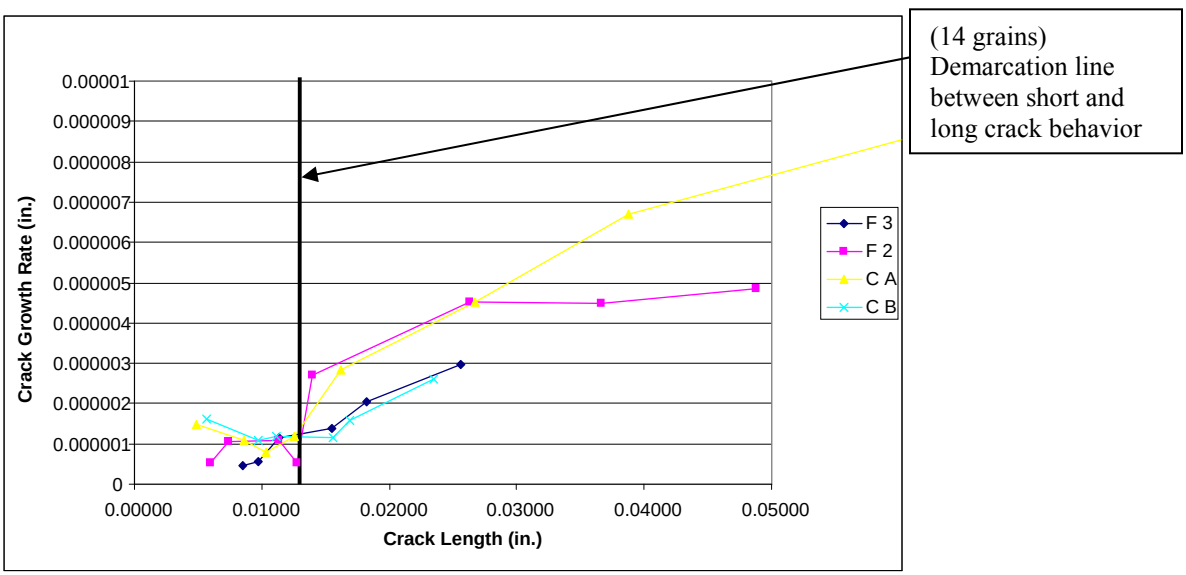

Figure 9. Crack Growth Rates in Both Small and Long Regimes

The difference in the behavior of primary and secondary cracks is shown in figure 10. This figure is the result of the distribution separation procedure that was applied to all measured cracks on a single specimen. The primary cracks are shown in red, and it is evident that their growth rates grow as they get larger. However, the growth rates of the secondary cracks, shown in multiple colors, tend to arrest. An example of the coalescence of two cracks, in this case both primary cracks, is also shown. The combined length of this coalesced crack reached a value much larger than any other crack on the specimen and led to failure long before failure was expected.

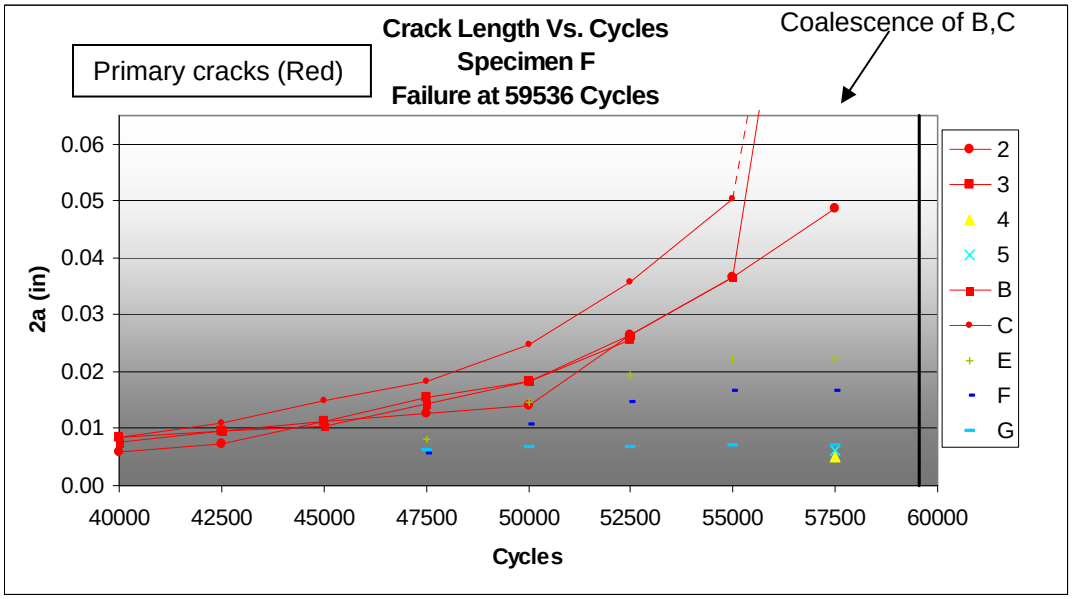

Figure 10. Crack Length vs Cycle Count for All Cracks Measured on Specimen F

3.5.2 Confidence Limit Analysis.

Meaningful confidence limits can only be calculated after the secondary cracks have been sorted away from the primary crack distribution. The reasons for this are shown below. In this analysis, confidence limits on the crack length versus cycle count were developed for all 14 of the primary cracks measured, including those that underwent coalescence.

Once the primary cracks were separated from the secondary crack distribution, it is easy to calculate the mean and standard deviation of the crack lengths at each cycle count where measurements were taken. The first step in the analysis was to determine a suitable distribution for these crack lengths at each cycle count. While the normal (Gaussian) distribution is extremely simple to work with, it is not appropriate because it would infer the existence of negative crack lengths. The normal distribution is also a symmetrical one, while the observed primary crack data is skewed, with emphasis on the larger tail due to several large cracks.

Related to the normal distribution, the lognormal distribution is not only simple to work with, but also offers a good approximation of the observed crack distributions. The utility of the lognormal distribution is that when it is transformed by the logarithm function, it becomes the normal distribution. This transformation and the resulting probability density function (PDF) of the lognormal distribution are shown in the following equations.

$$X \sim \text{Lognormal},\ Y \sim \text{Normal}$$
$$\ln(X) = Y \tag{4}$$

$$X(x) = \frac{1}{\sqrt{2\pi}\,\sigma x} e^{-(\ln(x)-\mu)^2/2\sigma^2} \tag{5}$$

$$E(X) = e^{\mu+\sigma^2/2} \tag{6}$$

$$Var(x) = e^{2\mu+\sigma^2}(e^{\sigma 2} - 1) \tag{7}$$

In these equations, μ and σ are the mean and standard deviation of the normal distribution associated with the lognormal distribution. The mean and variance for the lognormal distribution itself are shown for reference in equations 6 and 7, respectively.

With this assumption, the logarithm of all crack length data can be taken, thus giving data with a normal distribution. Confidence limits on the mean of this normal distribution can then be computed using the two-sided t-interval shown in the following equation.

$$\mu \in \left(\bar{x} - \frac{t_{\alpha/2,n-1} s}{\sqrt{n}}, \bar{x} + \frac{t_{\alpha/2,n-1} s}{\sqrt{n}} \right) \tag{8}$$

In the above equation, α is equal to one subtracted by the confidence limit. For all work contained herein, a confidence limit of 95% was used. The sample mean and standard deviation, given by $\bar{x}$ and *s*, are taken from the data that was transformed to come from the normal distribution. The number of crack measurements where the confidence limit is being built is represented by *n*. Finally, *t* represents the Student-t distribution with (n-1) degrees of freedom. Once the confidence limits on the mean of the normal distribution are found, the transformation is reversed on those limits, as shown in equation 9.

$$\nu \in \left(e^{\bar{x} - \frac{t_{\alpha/2,n-1} s}{\sqrt{n}}}, e^{\bar{x} + \frac{t_{\alpha/2,n-1} s}{\sqrt{n}}} \right) \tag{9}$$

This yields the 95% confidence limits on the mean of the crack lengths (ν) at the cycle count in which this analysis was completed.

The confidence limits on the mean of the crack lengths versus loading cycle was calculated, in the manner described above, for all primary cracks at each cycle count where measurements were taken. A plot of the primary crack data with the calculated confidence bounds is shown in figure 11.

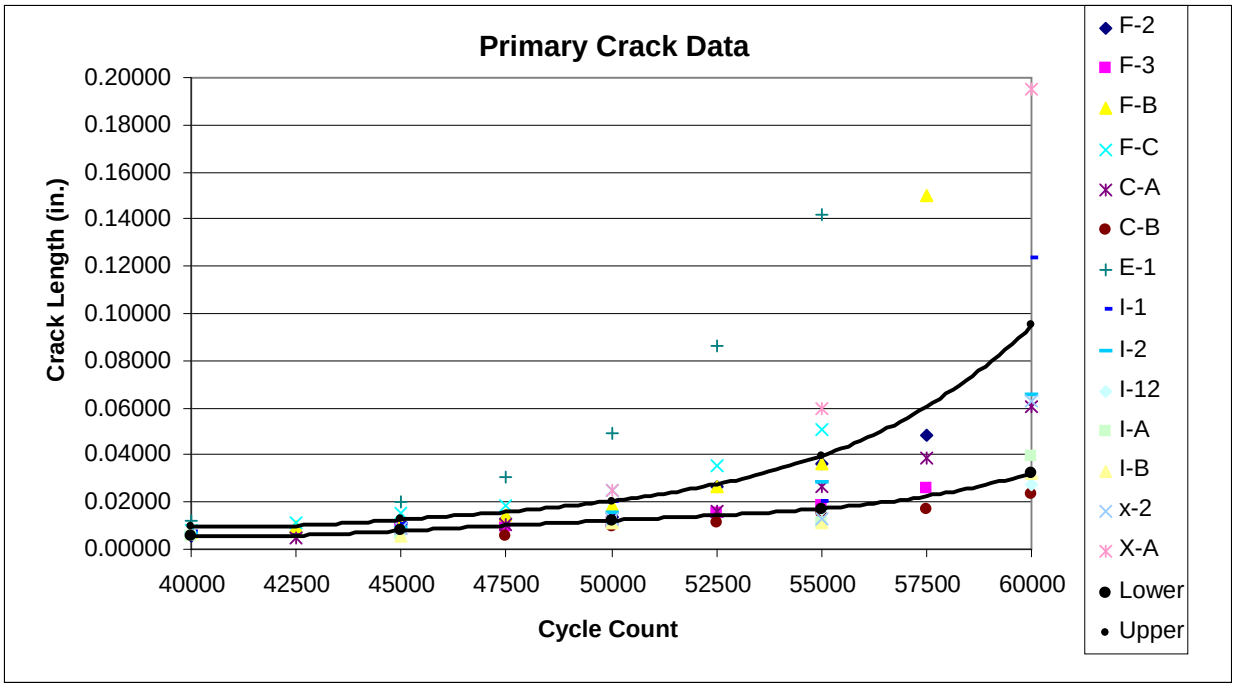

Figure 11. Confidence Bounds on the Mean of the Crack Lengths as Well as Primary Crack Data

In this figure, the multicolored points are the crack length data for the 14 primary cracks measured. The solid black lines are the calculated confidence limits on the mean. It is noted that a small number of cracks grew to very large lengths quickly and caused the positive skewness seen in the large upper bound. All cracks in this small subgroup grew to these lengths through crack coalescence. This highlights the importance of looking at clusters of cracks where coalescence is possible, rather than at single cracks where it cannot occur.

It should also be noted that the inclusion of secondary cracks will significantly and nonconservatively distort the calculated confidence limits. This would lead to unsafe predictions of fatigue life if these data were used for the design of a rotorcraft component. This is due to the fact that all 53 of the measured secondary cracks are smaller than the primary cracks at given cycle counts. To illustrate how these cracks will alter the confidence bounds, the new confidence bounds are shown in figure 12. This figure also shows the same primary crack data shown in figure 11, however, the secondary cracks have been removed for clarity.

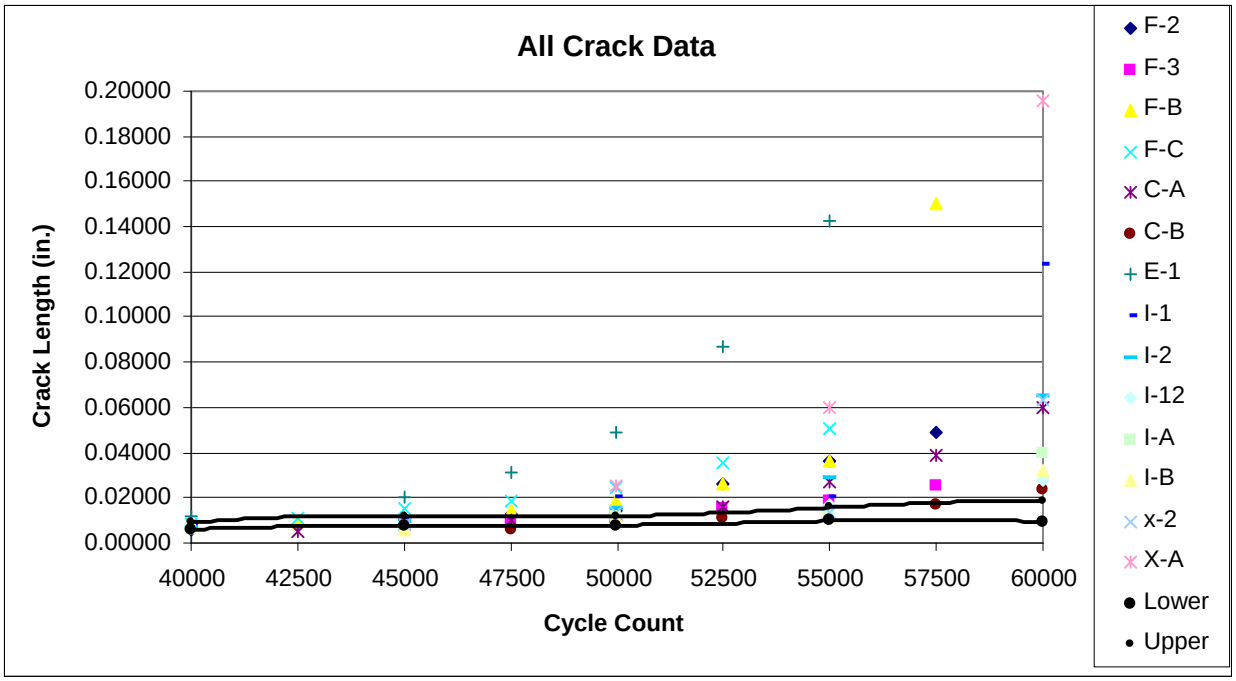

Figure 12. Confidence Bounds With the Inclusion of Secondary Cracks

3.5.3 Cluster Effects and Measurements.

In addition to crack length measurements, crack location measurements were recorded as well. This data allowed the crack cluster topology to be plotted and studied. An example of this is presented in figure 13. These plots show the evolution of crack clusters as they naturally initiate on 1 gage section of a specimen. Primary cracks are shown in red, and secondary cracks are shown blue. The plot area represents the gage section of the specimen. The axis is located vertically at the center of the specimen and horizontally at the left edge.

These topological measurements highlight the inherent complexity involved in any attempt to model a cluster of cracks because of the measured separations of the cracks in clusters. Many cracks are separated by relatively large distances where continuum methods apply. However, often cracks are separated by distances whose magnitude is on the order of the grain size of the material. The material in between these cracks may only contain a few grains and, thus, cannot be represented by an isotropic continuum. An exact analysis of this problem would quickly become intractable, therefore, statistical methods must be used for the problem of multisite cracking.

However, despite the complexity of the problem, some qualitative conclusions can be drawn from the crack cluster data. Many of the cracks, but not all, will be affected by other cracks through crack shielding and coalescence. A crack's driving force can either be raised or lowered due to the presence of a randomly arranged cluster around it. Therefore, the random crack clustering is an additional cause for the scatter seen in small crack growth. This effect continues to highlight the importance of approaching the problem of small fatigue crack growth using a nondeterministic approach applied to multisite growth.

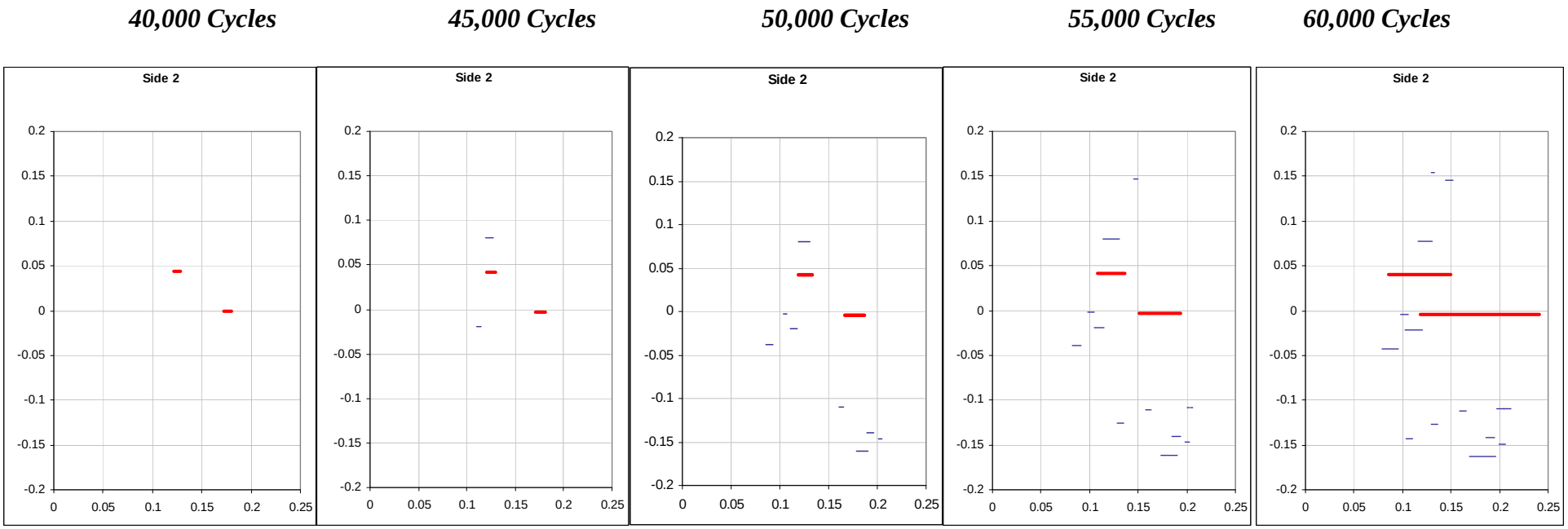

Figure 13. Topology of Multisite Crack Growth Through the Life of a Specimen

3.6 RECOMMENDATIONS FOR CONTINUING RESEARCH.

Future research in this area is needed to extend the results of the bimodal, statistical model developed in this project. This body of work can be divided into three areas: operational issues, analysis, and alternate materials.

3.6.1 Operational Issues.

In the experiments presented in this report, a constant-amplitude sinusoidal loading at a single *R*-ratio was applied to all specimens. However, during service, the components experienced variable amplitude loading. The effects of *R*-ratio should be investigated with additional constant-amplitude tests. Tests should also be conducted using industry-developed loading spectra. These tests would determine the effect of overloads and underloads on the growth of small fatigue cracks. The behavior of small cracks under such loading can be expected to differ from the behavior observed in long cracks, as growth acceleration/deceleration is a function of the size of the plastic zone [5]. The assumptions of small-scale yielding can then be violated for small cracks, which may be on the order of size as the plastic zone developed.

In addition to loading, the effect of material orientation should be studied. As shown previously in section 3.5.1, the microstructure of the plate form of material used in these experiments differed greatly depending on orientation. It can be expected that crack growth and transition behavior will also differ depending on orientation. Other forms of the material, such as rod or forging, can also be investigated.

Another aspect that should be studied is the effects of surface preparation. For all experiments performed for this project, specimens were polished to a 1-micron finish. However, rotorcraft components will not be prepared to these standards. Tests should be run with a representative surface preparation chosen collaboratively with industrial partners.

3.6.2 Analysis.

Along with additional testing, there is a significant body of analysis that would provide insight into the causes of scatter in small fatigue crack growth, and there are tools for the engineer to quantify this regime of growth. The effects of crack shielding can be quantified through the finite element method analysis of actual clusters measured during testing. Additionally, the use of statistically based stress-intensity factors that include physical parameters, such as grain size, should be investigated to quantify the growth of primary cracks.

3.6.3 Alternate Materials.

In addition to tests on aluminum alloys, beta-annealed Ti-6Al-4V should also be studied. This alloy is widely used in both the rotorcraft and fixed-wing industries. However, in this material, significant scatter is observed in the growth of both small and long cracks. This behavior may be a function of the complex microstructure found in this alloy.

Aluminum, being a single-phase material, will primarily have only a single microstructural parameter, the grain size. However, Ti-6Al-4V is a dual-phase metal with a complex

Widmänstatten-Colony type microstructure with several key parameters. These include the beta-grain size, the alpha-colony size within beta grains, and the width of the alpha lamellae. These features are primarily controlled by adjusting the rate at which the material is cooled during heat treatment and are often quite large. This explains the scatter of physically long cracks that may actually be microstructurally small. An example of how the microstructure can be altered by cooling rate is shown in figure 14.

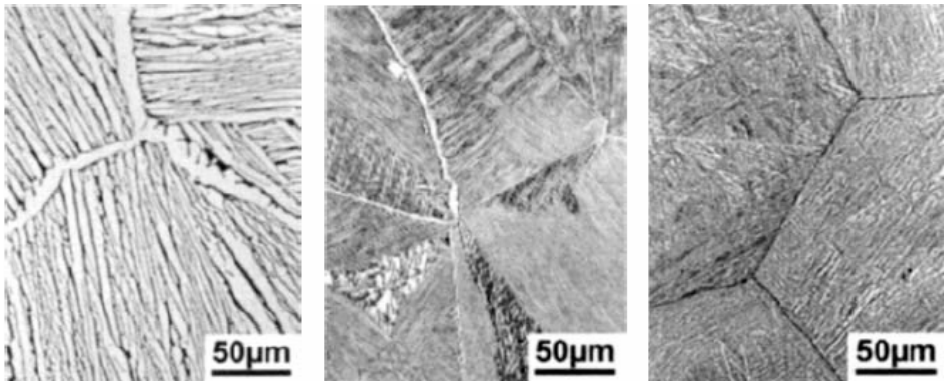

Figure 14. Microstructure of Ti-6Al-4V With Increased Cooling Rates and Finer Structures Towards the Right

4. CONCLUSIONS.

Based on the research results, it is concluded that:

- Many small cracks will take on nonstandard shapes such as forks and kinks. Several of these geometries may be the result of crack coalescence. The behavior of these cracks as they grow into large cracks must be continuously observed to assign a proper length for use in statistical analysis.

- A microstructurally based definition of the transition point between small and long crack growth has been applied successfully in two single-phase metallic materials. This point is defined as the crack length where the crack front will intersect an average of 14 grains.

- A bimodal statistical model was applied to micro-multi-site cracking. Behavioral differences were apparent between the secondary and primary crack distributions. It was shown that for analyses that would be used for crack prediction, only the primary crack distribution should be used, as inclusion of the secondary cracks would bias the results in a nonconservative direction.

- Crack coalescence was observed on approximately 1/6 of the observed specimen test surfaces. In many of these cases, this resulted in specimen failure at a cycle count well below what was expected had the cracks remained separate. These cases highlight the need to study cracks growing from smooth surfaces, rather than notches where only a single crack will form. In addition to crack coalescence, clusters of cracks were observed

to be close enough to lead to crack shielding. This additional micromechanism aids in explaining the observed scatter in the crack growth rates of small cracks.

- All the results contained in this report were for constant-amplitude loading, with a single *R*-ratio for aluminum alloy 7075-T7351. In the future, operational concerns, such as surface preparation, variable amplitude loading, and the effect of *R*-ratio, should be studied. In addition, the validity of the results obtained when applied to a dual phase alloy, such as Ti-6Al-4V, should be studied.

5. REFERENCES.

1. Schijve, J., "Fatigue of Structures and Materials," Kluwer Academic Publishers, Dordrecht, The Netherlands, 2001.

2. Chen, E.Y., Sauer, S., Meshii, M., and Tucker, W.T., "Fatigue Micro Crack Distributions and the Reliability of a Nickel Base Super Alloy," *International Journal of Fatigue*, 1997, pp. 75-82.

3. Stolarz, J. and Kurzydlowski, "Stereological Analysis of Fatigue Short Crack Propagation in Zicolloy-4," *Fourth Int. Conf. on Low Cycle Fatigue and Elasto-Plastic Behavior of Materials*, 1998, pp. 535-540.

4. Swain, M.H., "Monitoring Small-Crack Growth by the Replication Method," *Small-Crack Test Methods, ASTM STP 1149*, Larsen, J.M. and Allison, J.E., eds., 1992, pp. 34-56.

5. Carlson, R.L. and Kardomateas, G.A., "Effects of Compressive Load Excursions on Fatigue Crack Growth," *International Journal of Fracture*, Vol. 16, 1994, pp. 141-146.

6. Carlson, R.L., "An Examination of Scatter in Small Fatigue Crack Growth," *International Journal of Fracture*, Vol. 115, 2002, pp. 55-60.

7. Detter-Hoskin, L. and Patel, G., "Measurements of Particle Size and Grain Size in Al 7075 Hot-Rolled Sample," GTRI Sub Project No. A7542-000, 2004.

8. Young, W.C., Budynas, R., and Roark, R., "Roark's Formulas for Stress and Strain," *McGraw Hill Professional*, USA, 2001.